Fast Tunable Coupler for Superconducting Qubits

R. C. Bialczak,[1] M. Ansmann,[1] M. Hofheinz,[1] M. Lenander,[1] E. Lucero,[1] M. Neeley,[1] A. D. O'Connell,[1] D. Sank,[1] H. Wang,[1] M. Weides,[1] J. Wenner,[1] T. Yamamoto,[2] A. N. Cleland,[1] and J. M. Martinis[1,*]

[1]*Department of Physics, University of California, Santa Barbara, California 93106, USA*

[2]*Green Innovation Research Laboratories, NEC Corporation, Tsukuba, Ibaraki 305-8501, Japan*

(Received 15 September 2010; published 9 February 2011)

A major challenge in the field of quantum computing is the construction of scalable qubit coupling architectures. Here, we demonstrate a novel tunable coupling circuit that allows superconducting qubits to be coupled over long distances. We show that the interqubit coupling strength can be arbitrarily tuned over nanosecond time scales within a sequence that mimics actual use in an algorithm. The coupler has a measured on/off ratio of 1000. The design is self-contained and physically separate from the qubits, allowing the coupler to be used as a module to connect a variety of elements such as qubits, resonators, amplifiers, and readout circuitry over distances much larger than nearest-neighbor. Such design flexibility is likely to be useful for a scalable quantum computer.

DOI: 10.1103/PhysRevLett.106.060501 PACS numbers: 03.67.Lx, 85.25.Cp

Researchers using superconducting qubits have made significant progress towards building a simple quantum computer [1,2]. However, as superconducting circuits become more complex, with larger numbers of qubits, the fidelity of quantum algorithms will begin to be dominated by unwanted qubit interactions, increased decoherence, and frequency-crowding, all inherent to traditional frequency-tuned architectures [3–5]. Tunable coupling between qubits may provide a solution, as this would allow the direct control of qubit interactions, with large "on" coupling consistent with very small to zero "off" coupling [3,4], without introducing nonidealities that limit performance. Tunable couplers have been demonstrated using superconducting qubits [6–9], but only using designs that require the tuning element to be in close proximity to the qubits, and have shown either limited time-domain control or low on-to-off ratios, thus providing a proof-of-concept, but limited in scalability and performance. Here we present a design which, for the first time in a single device, achieves nanosecond time resolution with a large on-to-off-coupling ratio. The design is completely modular, allowing coupling of qubits across large distances, not just nearest neighbors and permitting coupling to other superconducting circuit elements, likely necessities for assembling a quantum computer. We demonstrate use of the coupler in a sequence of gate operations that mimic actual use in an algorithm.

The electrical circuit for the coupled Josephson phase qubits [5,10,11] is shown in Fig. 1(a) and a corresponding optical micrograph is shown in Figs. 1(b)–1(f). Each phase qubit [Figs. 1(b) and 1(c)] is a nonlinear resonator built from an $Al/AlO_x/Al$ Josephson junction with critical current $I_0 = 1.6\ \mu A$, and external shunting capacitors and inductors, $C = 1$ pF and $L = 750$ pH. When biased close to the critical current, the junction and its parallel loop inductance L give rise to a cubic potential whose energy eigenstates are unequally spaced. The two lowest levels are used as the qubit states $|0\rangle$ and $|1\rangle$, with transition frequency $\omega_{10}/2\pi$. Logic operations (X and Y rotations) are

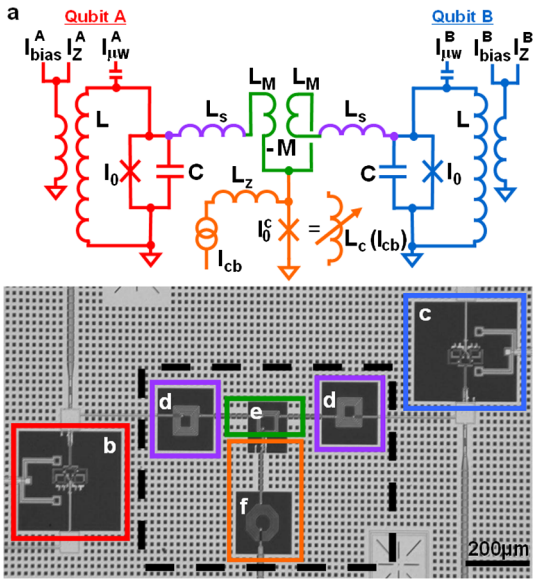

FIG. 1 (color online). Device circuit and micrograph of two Josephson phase qubits with a tunable coupler. The two qubits are shown in red and blue in the circuit, and boxes b and c in the lower micrograph, and are described in detail elsewhere [5,10,11,15]. The inductors L_s, L_M, and the mutual inductance M, which form the nontunable part of the coupler, are shown in purple and green, and boxes d and e. The current-biased coupler junction, which forms the tunable element, is shown in orange and in box f. The inductor $L_z = 9$ nH isolates the coupler from the bias circuit. The entire coupler, a modular four-terminal device, is shown by the dashed box. The coupler wiring can be made longer, if needed, to connect qubits over greater distances.

performed by applying microwave pulses $I_{\mu W}^{A,B}$ at this transition frequency, whereas changes in frequency (Z rotations) and measurement are produced by ~ns pulses in the bias current $I_Z^{A,B}$ [5,10,11].

The tunable coupling element [Fig. 1(d)–1(f)] is a four-terminal device constructed using a fixed negative mutual inductance $-M$ [Fig. 1(e)] and a single, current-biased Josephson junction [Fig. 1(f)] that acts as a tunable positive inductance L_c. This inductance changes with coupler bias $I_{\rm cb}$ according to [12], $L_c = (\Phi_0/2\pi I_0^c)/\sqrt{1-(I_{\rm cb}/I_0^c)^2}$ where $I_0^c \simeq 1.58\ \mu$A is the coupler junction critical current. The interaction Hamiltonian between qubits A and B for the tunable coupler is [3]

$$H_{\rm int} \simeq \frac{\hbar\Omega_c}{2}\left(\sigma_{x,A}\sigma_{x,B} + \frac{1}{6\sqrt{N_A N_B}}\sigma_{z,A}\sigma_{z,B}\right) \quad (1)$$

with

$$\Omega_c = \frac{M - L_c}{(L_M + L_s)^2 \omega_{10} C}, \quad (2)$$

where σ is the Pauli operator, N is the normalized well depth, and $\Omega_c \propto M - L_c$ is the adjustable coupling strength [3].

The direct connection of the qubits through this circuit allows for strong coupling. To reduce the coupling magnitude to the desired 50 MHz range, series inductors $L_s \simeq 2700$ pH [Fig. 1(d)] are inserted in the connecting wires that are significantly larger than for the mutual inductance element $L_M \simeq 390$ pH and $M \simeq 190$ pH. Because the number of levels in the potentials of qubits A and B are typically $N_A = N_B \simeq 5$, the $\sigma_{z,A}\sigma_{z,B}$ term in Eq. (1) gives a small contribution of approximately 0.03 to the coupling strength. This interaction does not affect the results presented here and can be effectively removed using a simple refocusing sequence if needed. With parameters $I_0^c \simeq 1.58\ \mu$A and $M = 190$ pH, and full adjustment of the bias current, coupling strengths $\Omega_c/2\pi$ were varied from approximately 0 to 100 MHz. The values of I_0^c and M can be chosen so that other ranges of coupling strength, both positive and negative in sign, are possible.

The direct-current connections between the coupler bias and the qubits produce small shifts in the qubit frequency due to changes in the coupler bias. These shifts can be readily compensated for using the qubit biases $I_Z^{A,B}$ and are discussed in the supplementary information [13], along with a coupler reset protocol [14].

The coupler can be operated in two modes. In the simplest "static" mode, the coupler is held at a fixed strength throughout a two-qubit pulse sequence. A more realistic "dynamic" mode uses a fast nanosecond-scale pulse to turn the coupler on and off during a control sequence that contains both single and two-qubit operations and measurement.

Using the static mode, we performed spectroscopy at a fixed coupler bias, which allowed us to measure the energy splitting $\Omega_c/2\pi$ at the avoided level crossing where the detuning $\Delta/2\pi = f_{0A} - f_{0B}$ between the two qubits was zero. The pulse sequence for this experiment is shown in Fig. 2(a). The coupler bias (green) is set to the value $I_{\rm cb}$, and is kept at this constant value throughout this static experiment. The dashed line indicates the coupler bias level that corresponds to zero coupling strength, $\Omega_c/2\pi \simeq 0$ MHz. The qubits (red and blue) are initially detuned by 200 MHz and each starts in the $|0\rangle$ state. The bias of qubit B is then adjusted to set its transition frequency a distance $\delta/2\pi$ from the qubit A frequency, f_{0A}. A microwave pulse of frequency $f_{\mu W}$ and duration ~2 μs is then applied to each qubit. Both qubit states are then determined using a single-shot measurement. A representative subset of crossings for several coupler biases are shown in Figs. 2(b)–2(e). The coupler clearly modulates the size of the spectroscopic splitting, and allows the setting and measuring of the coupling strength [3,10,15]. Although the data for 0 MHz show no apparent splitting, the resolution at zero coupling is limited to ± 1.5 MHz by the 3 MHz linewidth, which is slightly power broadened. Submegahertz resolution of the minimum coupling strength is obtained from the time-domain experiments, as discussed below.

Since the fidelity of gate operations is limited by qubit coherence times [10], we want to reduce gate times by using strong coupling. For devices with fixed capacitive

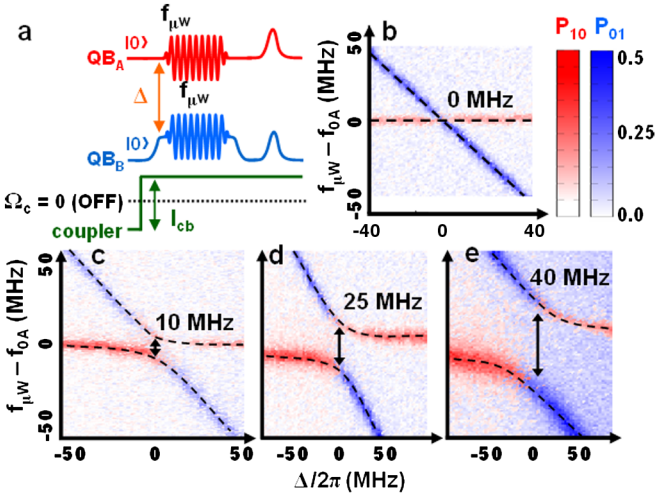

FIG. 2 (color online). Tuning the spectroscopic splitting. (a) Pulse sequence for qubit spectroscopy, as described in the text. The panels (b)–(e) are plots of the measured probability P_{10} (A excited) and P_{01} (B excited) versus the detuning frequency $\Delta/2\pi$ and the difference in microwave and qubit A frequencies $f_{\mu W} - f_{0A}$. Each panel shows a different coupler bias $I_{\rm cb}$ that increases from (b)–(e) The splitting size, $\Omega_c/2\pi$ measured as the minimum distance between the two resonance curves, shows the coupling strength being adjusted by the coupler. The dotted lines are a guide to the eye.

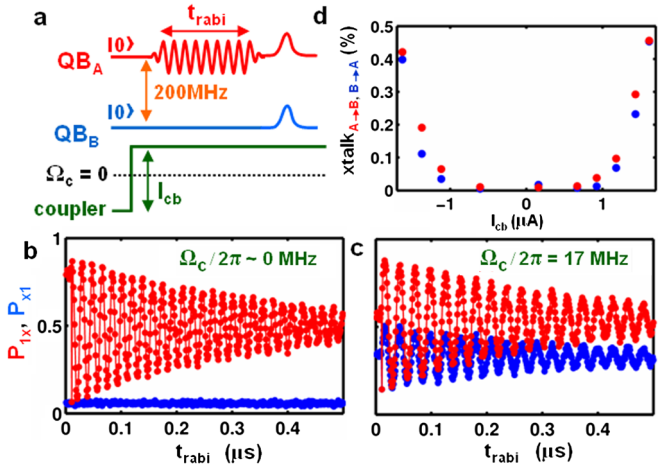

FIG. 3 (color online). Turning off measurement cross talk. (a) Pulse sequence for determining the measurement cross talk as a function of coupler bias, as described in the text. (b) For the tunable coupler turned off, we plot $P_{x1} = P_{01} + P_{11}$ and $P_{1x} = P_{10} + P_{11}$ versus the Rabi pulse time t_{rabi}. Rabi oscillations in P_{1x} (qubit A) are observed, with only a small amplitude oscillation of P_{x1} (qubit B) coming from measurement cross talk. (c) Same as for (b), but with coupling turned on to 17 MHz. (d) Measurement cross talk amplitude as a function of coupler bias I_{cb} for the case of Rabi drive on qubit A (red) and qubit B (blue). For the case of drive on qubit A (qubit B), cross talk amplitude is displayed as the ratio of the amplitudes of the oscillations of $P_{x1}(P_{1x})$ to that of $P_{1x}(P_{x1})$.

coupling, however, this strategy cannot be used effectively because of the rapid rise in measurement cross talk with increased coupling [15,16]. Therefore, it is important to demonstrate that measurement cross talk can be reduced to a minimal value when the coupler is turned off. As shown in Fig. 3(a), we determine measurement cross talk by driving only one qubit with Rabi oscillations, and then simultaneously measuring the excitation probabilities of both qubits [16]. The coupler (green) is set to a static bias I_{cb}. The coupler bias level corresponding to zero coupling strength, $\Omega_c/2\pi \simeq 0$ MHz, is indicated by the dashed line. The qubits remain detuned by 200 MHz throughout the experiment, and only one qubit (shown here, A) is excited with microwaves. The undriven qubit ideally shows no response, with the ratio of the amplitudes of the oscillations giving a quantitative measure of the measurement cross talk. The Rabi data are shown in Figs. 3(b) and 3(c) for both the driven and undriven qubits, using representative coupling strengths of 0 and ~17 MHz. The measurement cross talk is plotted as a function of coupler bias in Fig. 3(d), where there is a broad region of coupler bias where the measurement cross talk amplitude is minimized. This tunable coupler allows operation of phase qubits at large coupling strengths without the drawback of large measurement cross talk.

The dynamic mode of operation tests coupler performance with a sequence that mimics actual use in an algorithm. This pulse sequence is illustrated in Fig. 4(a). The coupler (green) is first set to the coupler bias value corresponding to $\Omega_c/2\pi \simeq 0$ MHz, as measured previously. The qubits (red and blue) are initially detuned by $\Delta/2\pi = 200$ MHz and start in the $|0\rangle$ state. A π microwave pulse is then applied to qubit A, exciting it to the $|1\rangle$ state. The coupling interaction remains off during this pulse to minimize errors resulting from two-qubit interactions. A fast bias pulse then detunes qubit B from qubit A by a frequency $\Delta/2\pi$, and at the same time compensates for qubit bias shifts due to the coupler. Simultaneously, the coupler is turned on to a bias I_{cb} using a fast bias pulse with ~2 ns rise and fall times. The coupler and qubit biases are held at these values for a time t_{swap}, allowing the two-qubit system to evolve under the coupling interaction. The coupling produces a two-qubit swap operation which arises from the $\sigma_x\sigma_x$ operator in Eq. (1), which is the basis for universal gate operations [10]. The qubits are then detuned again to $\Delta/2\pi = 200$ MHz and I_{cb} is set back to zero coupling strength, allowing for a cross talk-free single-shot measurement of the two-qubit probabilities $P_{AB} = \{P_{01}, P_{10}, P_{11}\}$.

In Fig. 4(b), we show swap data for two representative settings for on and off coupling, $\Delta/2\pi \simeq 0$ MHz at $\Omega_c/2\pi \simeq 0$ and 40 MHz. In Fig. 4(c), swap data are shown where the detuning, $\Delta/2\pi$ was varied for several representative coupling strengths $\Omega_c/2\pi \simeq 0$, 11, 27, 45, and 100 MHz. The swaps exhibit the expected chevron pattern for the resonant interaction [15]. In Fig. 4(d) the swap frequency is plotted versus coupler bias for $\Delta/2\pi \simeq 0$ MHz. Coupling strengths up to 100 MHz are possible, although we find that the decay times of the swaps degrade above 60 MHz, presumably due to the coupler bias approaching the critical current of the coupler junction.

The determination of the minimum coupling strength, which quantifies how well the interaction can be turned off, is limited by the minimum detectable swap frequency of the qubits. This frequency, in turn, is limited by qubit decoherence. A comparison of the off-coupling data in Fig. 4(b) to simulations (see supplementary information [13]) shows that the smallest resolvable coupling strength is no greater than 0.1 MHz. Given this upper bound on the minimum coupling strength, the measured on/off ratio for the swap interaction is approximately 100 MHz/0.1 MHz = 1000.

Stray capacitances and inductances in the circuit introduce stray coupling that may limit the on/off ratio. In this design, the greatest contribution to stray coupling comes from the small, inherent capacitance of the coupler junction. The coupler junction has a self-resonance frequency of $\omega_{c0}/2\pi \simeq 30$ GHz, which implies that its effective inductance $L_c[1 - (\omega/\omega_{c0})^2]$ changes in value from $\omega/2\pi = 0$ and 6 GHz by ~4% [3]. The $\sigma_z\sigma_z$ and $\sigma_x\sigma_x$ interactions in Eq. (1) will thus turn on and off at slightly different biases and, along with virtual transitions, will limit how far the coupler can be turned off [3,4]. A useful

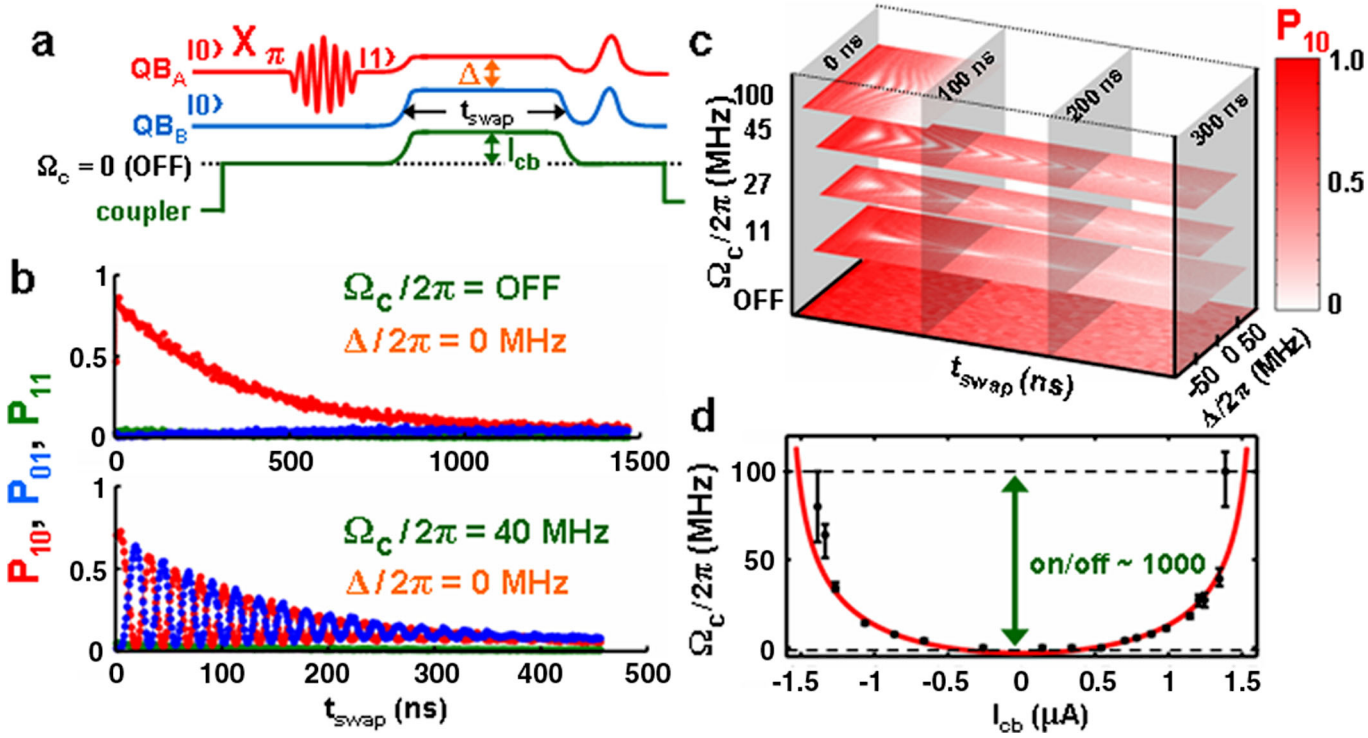

FIG. 4 (color online). Demonstration of dynamic coupler operation via swap experiment. (a) Pulse sequence demonstrating dynamic mode of coupler operation, as described in the text. (b) The measured two-qubit probabilities P_{01}, P_{10}, and P_{11} are plotted versus t_{swap} for qubits on resonance $\Delta/2\pi = 0$ and two sets of coupling $\Omega_c/2\pi$, corresponding to off (top) and on (bottom) conditions. (c) Measured qubit probability, P_{10}, plotted versus t_{swap} and qubit detuning $\Delta/2\pi$ for representative coupling strengths $\Omega_c/2\pi = 0$, 11, 27, 45, and 100 MHz. (d) Swap frequency $\Omega_c/2\pi$ versus coupler bias I_{cb} for all coupler biases measured in this experiment (solid dots). Solid red line is theory obtained from Eq. (2) and measured device parameters.

feature of this coupler is that this imperfection can be compensated for by including a small shunt capacitor across the mutual inductance [3], which should allow on/off ratios up to 10^4.

The performance of this coupler, especially its ability to strongly couple qubits over long distances, makes it a promising "drop-in" module for scalable qubit architectures. The demonstration of coupling adjustment over nanosecond time scales, along with a large on/off ratio allows the implementation of algorithms that require on-the-fly tuning of the coupling strength [17]. We also foresee the use of this coupling circuit in other applications, such as superconducting parametric amplifiers [18] or in coupling qubits to readout circuitry, superconducting resonators, or other circuit elements.

Devices were made at the UCSB Nanofabrication Facility, a part of the NSF-funded National Nanotechnology Infrastructure Network. We thank A. N. Korotkov, R. A. Pinto, and M. R. Geller for discussions. This work was supported by IARPA (grant W911NF-04-1-0204) and by the NSF (grant CCF-0507227).

*martinis@physics.ucsb.edu

[1] T. D. Ladd *et al.*, Nature (London) **464**, 45 (2010).
[2] B. G. Levi, Phys. Today **62**, No. 7, 14 (2009).
[3] R. A. Pinto *et al.*, Phys. Rev. B **82**, 104522 (2010).
[4] S. Ashhab *et al.*, Phys. Rev. B **77**, 014510 (2008).
[5] J. M. Martinis, Quant. Info. Proc. **8**, 81 (2009).
[6] T. Hime *et al.*, Science **314**, 1427 (2006).
[7] A. O. Niskanen *et al.*, Science **316**, 723 (2007).
[8] M. Allman *et al.*, Phys. Rev. Lett. **104**, 177004 (2010).
[9] R. Harris *et al.*, Phys. Rev. Lett. **98**, 063602 2007).
[10] R. C. Bialczak *et al.*, Nature Phys. **6**, 409 (2010).
[11] M. Steffen *et al.*, Science **313**, 1423 (2006).
[12] A. Barone and G. Paterno, *Physics and Applications of the Josephson Effect* (John Wiley & Sons, New York, 1982).
[13] See supplemental material at http://link.aps.org/supplemental/10.1103/PhysRevLett.106.060501.
[14] T. A. Palomaki *et al.*, Phys. Rev. B **73**, 014520 (2006).
[15] R. McDermott *et al.*, Science **307**, 1299 (2005).
[16] M. Ansmann *et al.*, Nature (London) **461**, 504 (2009).
[17] A. Galiautdinov and M. Geller, arXiv:quant-ph/0703208.
[18] N. Bergeal *et al.*, Nature (London) **465**, 64 (2010).